Supplementary information

Phase stability and fast ion transport in P2-type layered Na$_2$X$_2$TeO$_6$ (X = Mg, Zn) solid electrolytes for sodium batteries

He Huang[1], Yuewang Yang[1], Cheng Chi[1], Hong-Hui Wu[2], and Baoling Huang[1,3*]*

[1] Department of Mechanical and Aerospace Engineering, The Hong Kong University of Science and Technology, Clear Water Bay, Hong Kong SAR, China

[2] School of Materials Science and Engineering, University of Science and Technology Beijing, Beijing, 100083, China

[3] The Hong Kong University of Science and Technology Foshan Research Institute for Smart Manufacturing, Guangzhou, Guangdong, China

* Corresponding authors. E-mail address: mebhuang@ust.hk (B. Huang), wuhonghui@ustb.edu.cn (H.-H. Wu)
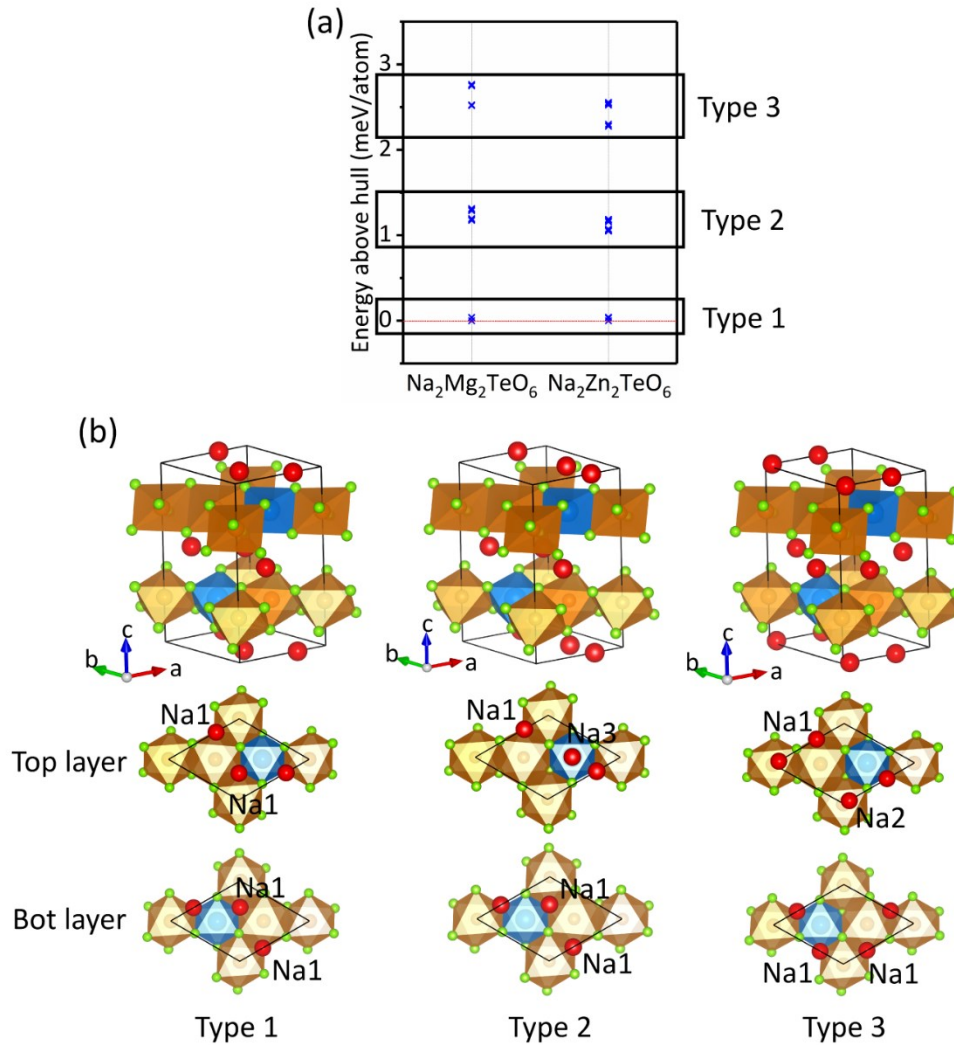
Figure S1. (a) Energies above the hulls of NMTO and NZTO with 20 different configurations at relatively low electrostatic energies enumerated by Ewald enumeration method. According to the energy distribution in Figure S1(a), three typical configuration types are listed: Type 1, Type 2, and Type 3. (b) The optimized structural configurations with the lowest energies in Type 1 (left), Type 2 (middle), and Type 3(right). The orange octahedra present $Mg(Zn)O_{6/3}$, and the blue octahedra present $TeO_{6/3}$. The red balls represent occupied Na atoms. To have better visions, the Na ion distribution configurations on the top and bottom layers of NMTO and NZTO are separately shown. It shows that Na ions prefer to locate in Na1 sites, then Na3 sites and Na2 sites.
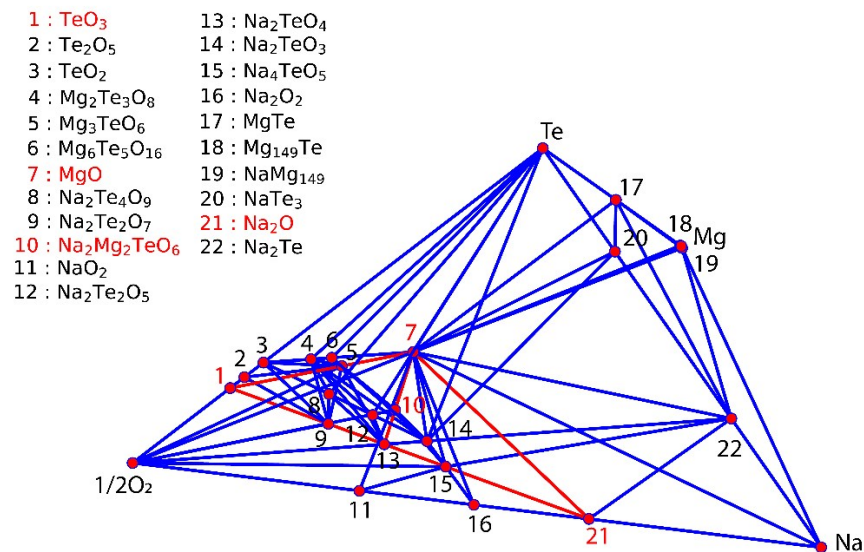
1 : TeO$_3$ 13 : Na$_2$TeO$_4$
2 : Te$_2$O$_5$ 14 : Na$_2$TeO$_3$
3 : TeO$_2$ 15 : Na$_4$TeO$_5$
4 : Mg$_2$Te$_3$O$_8$ 16 : Na$_2$O$_2$
5 : Mg$_3$TeO$_6$ 17 : MgTe
6 : Mg$_6$Te$_5$O$_{16}$ 18 : Mg$_{149}$Te
7 : MgO   19 : NaMg$_{149}$
8 : Na$_2$Te$_4$O$_9$ 20 : NaTe$_3$
9 : Na$_2$Te$_2$O$_7$ 21 : Na$_2$O
10 : Na$_2$Mg$_2$TeO$_6$ 22 : Na$_2$Te
11 : NaO$_2$
12 : Na$_2$Te$_2$O$_5$

Figure S2. Grand state DFT calculated quaternary Na-Mg-Te-O phase diagram at 0 K and 0 atm. The red dots represent all calculated stable decomposition compounds. The NMTO phase is found stable in the ternary phase diagram with the given compounds Na$_2$O, MgO, and TeO$_3$ as the three vertices of the diagram triangles (red triangle shown in the figure).
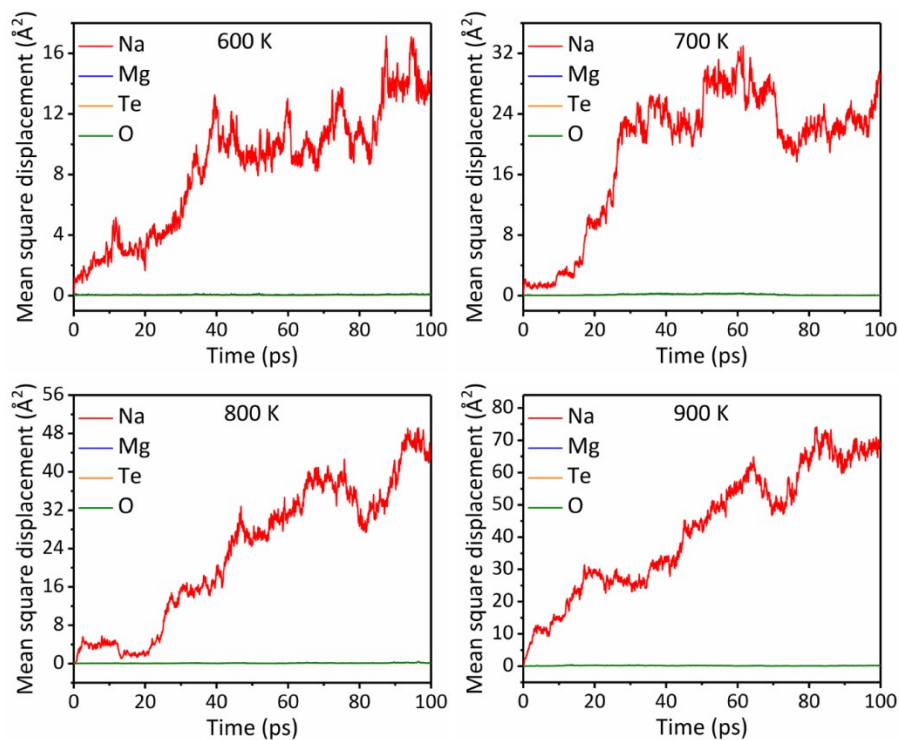
Figure S3. Mean square displacements of NMTO versus time scale with the temperature
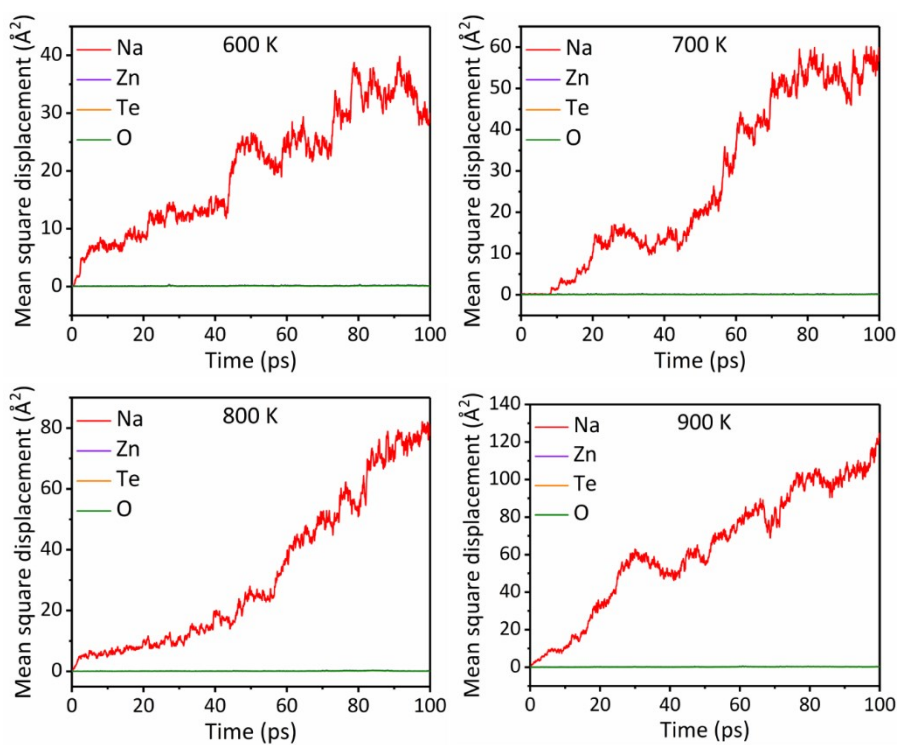
3

range from 600 K to 900 K.

Figure S4. Mean square displacements of NZTO versus time scale with the temperature range from 600 K to 900 K.
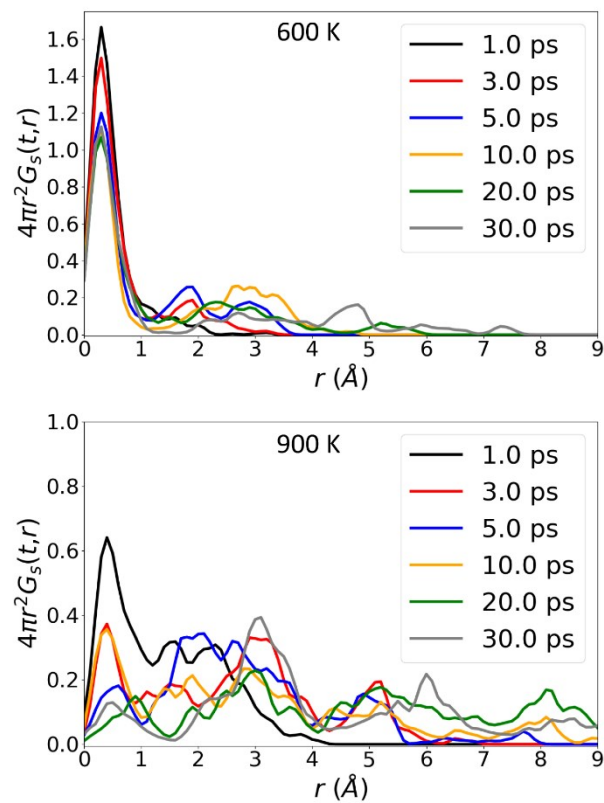
Figure S5. Self-part of the van Hove correlation function of NMTO at 600 K and 900 K. The correlation evolution is illustrated by five different time points: 1 ps, 3 ps, 5 ps, 10 ps, 20 ps and 30 ps.
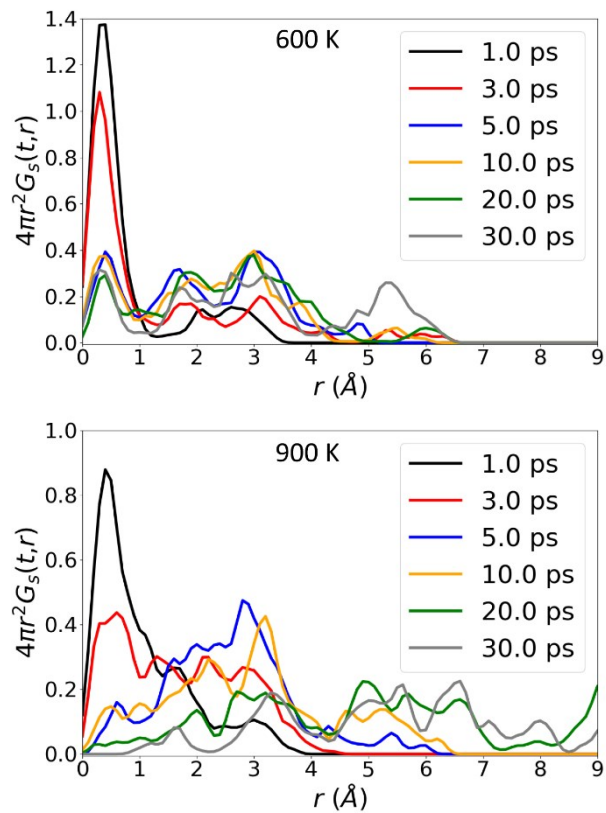
Figure S6. Self-part of the van Hove correlation function of NZTO at 600 K and 900 K. The correlation evolution is illustrated by five different time points: 1 ps, 3 ps, 5 ps, 10 ps, 20 ps and 30 ps.
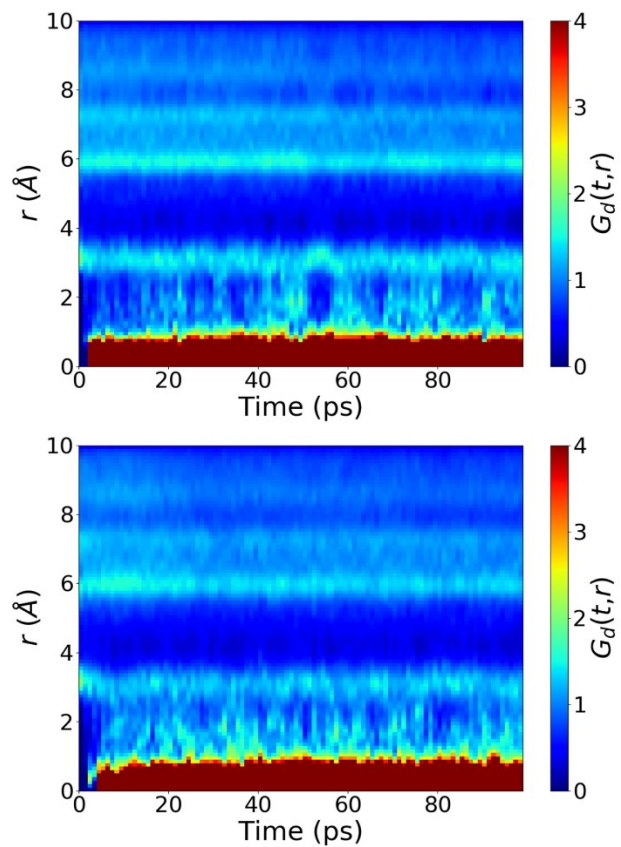
Figure S7. Distinct parts of the van Hove correlation function of NMTO (top) and NZTO (bottom) at 900 K along the whole simulations.
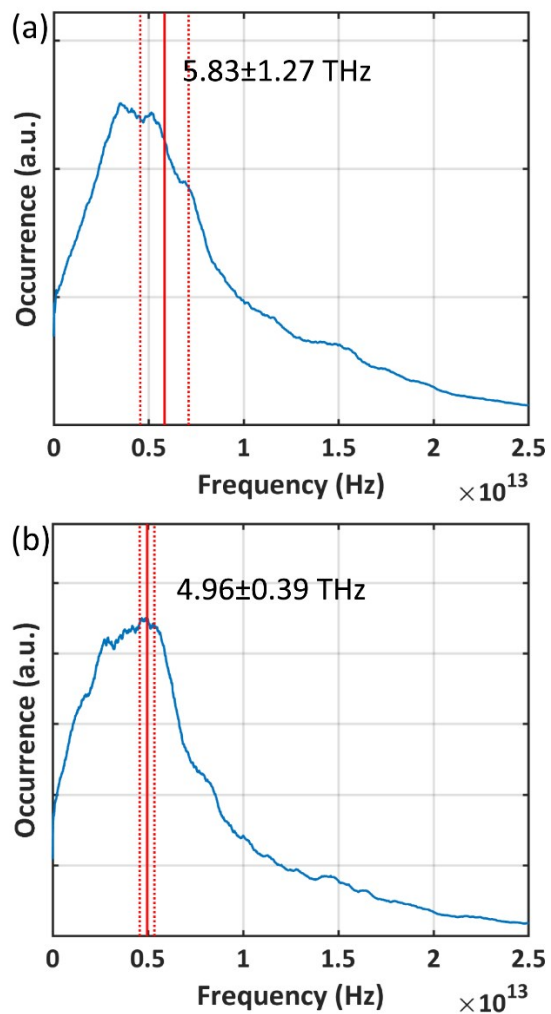
Figure S8. Vibration frequency spectrums of Na ions in (a) NMTO and (b) NZTO at 800 K. The average vibration frequency and relevant standard variance are shown by the solid (± dotted) red line.
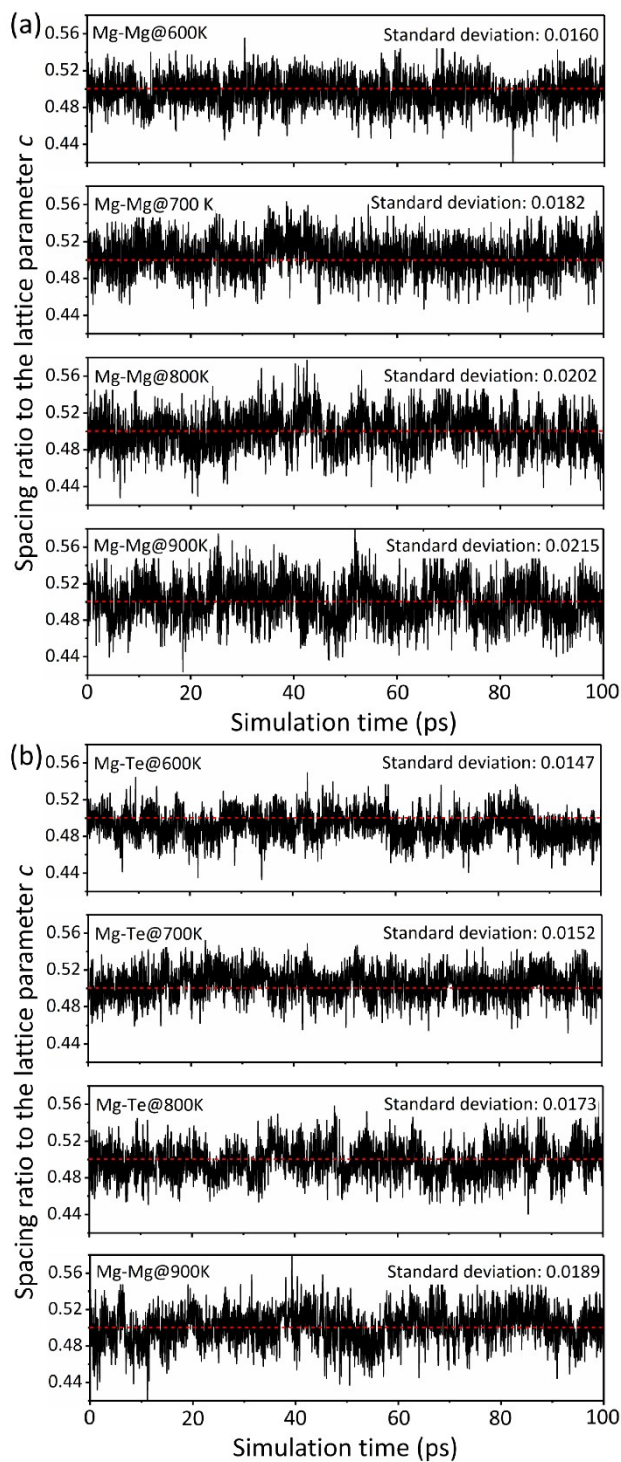
Figure S9. Interlayer (a) Mg-Mg and (b) Mg-Te spacing ratios to the lattice parameter *c* of NMTO in the AIMD simulations from 600 K to 900 K. The corresponding standard deviation values are shown in the inserted captions.
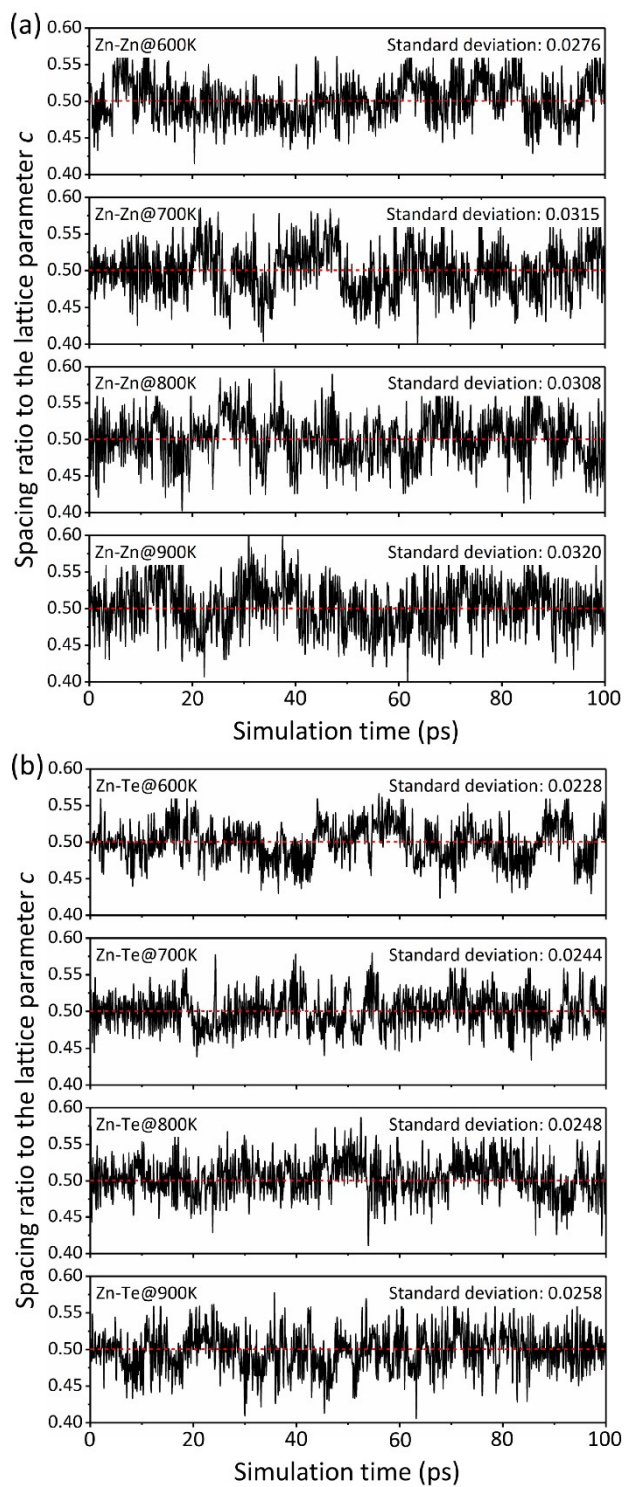
Figure S10. Interlayer (a) Zn-Zn and (b) Zn-Te spacing ratios to the lattice parameter *c* of NZTO in the AIMD simulations from 600 K to 900 K. The corresponding standard deviation values are shown in the inserted captions.

Table S1. Chemical reactions of NMTO and NZTO upon the sodium uptake or extraction at different calculated voltages.

	Voltage (V)	Chemical reaction
NMTO	0.0	$2Na_2Mg_2TeO_6 + 16Na \rightarrow 8Na_2O + 2Na_2Te + 4MgO$
	0.68	$2Na_2Mg_2TeO_6 + 3.2Na \rightarrow 1.6Na_4TeO_5 + 0.4Na_2Te + 4MgO$
	1.05	$2Na_2Mg_2TeO_6 + 2Na \rightarrow Na_4TeO_5 + Na_2TeO_3 + 4MgO$
	1.74	$2Na_2Mg_2TeO_6 \rightarrow 2Na_2Mg_2TeO_6$
	3.15	$2Na_2Mg_2TeO_6 \rightarrow 0.6667Na_2TeO_4 + 1.333Mg_3TeO_6 + 0.6667O_2 + 2.667Na$
	3.44	$2Na_2Mg_2TeO_6 \rightarrow 0.3333Na_2Te_2O_7 + 1.333Mg_3TeO_6 + 0.8333O_2 + 3.333Na$
	3.90	$2Na_2Mg_2TeO_6 \rightarrow 0.6667TeO_3 + 1.333Mg_3TeO_6 + O_2 + 4Na$
	Voltage (V)	**Chemical reaction**
NZTO	0.0	$2Na_2Zn_2TeO_6 + 24.31Na \rightarrow 0.3077NaZn_{13} + 12Na_2O + 2Na_2Te$
	0.11	$2Na_2Zn_2TeO_6 + 18.08Na \rightarrow 3Na_6ZnO_4 + 0.07692NaZn_{13} + 2Na_2Te$
	0.25	$2Na_2Zn_2TeO_6 + 16Na \rightarrow 0.5714Na_{10}Zn_4O_9 + 1.714Na_6ZnO_4 + 2Na_2Te$
	0.73	$2Na_2Zn_2TeO_6 + 11.2Na \rightarrow Na_{10}Zn_4O_9 + 1.4Na_2Te + 0.6Na_4TeO_5$
	0.78	$2Na_2Zn_2TeO_6 + 9.6Na \rightarrow 4Na_2ZnO_2 + 1.2Na_2Te + 0.8Na_4TeO_5$
	0.84	$2Na_2Zn_2TeO_6 + 6.4Na \rightarrow 2Na_2Zn_2O_3 + 0.8Na_2Te + 1.2Na_4TeO_5$
	0.99	$2Na_2Zn_2TeO_6 + 3.2Na \rightarrow 0.4Na_2Te + 1.6Na_4TeO_5 + 4ZnO$
	1.05	$2Na_2Zn_2TeO_6 + 2Na \rightarrow Na_2TeO_3 + Na_4TeO_5 + 4ZnO$
	2.25	$2Na_2Zn_2TeO_6 \rightarrow 2Na_2TeO_4 + 4ZnO$
	3.23	$2Na_2Zn_2TeO_6 \rightarrow 0.6667Na_2TeO_4 + 1.333Zn_3TeO_6 + 0.6667O_2 + 2.667Na$
	3.44	$2Na_2Zn_2TeO_6 \rightarrow 1.333Zn_3TeO_6 + 0.3333Na_2Te_2O_7 + 0.8333O_2 + 3.333Na$
	3.90	$2Na_2Zn_2TeO_6 \rightarrow 1.333Zn_3TeO_6 + 0.6667TeO_3 + O_2 + 4Na$

Table S2. Mean jump rate (Γ), total jump diffusivity (D_J) of NMTO and NZTO in comparison to the tracer diffusivity (D^*) calculated by AIMD simulations at different

temperatures (T) from 600 K to 900 K.

	T	Jump rate ($\times 10^{10}$ s^{-1})	Jump diffusivity (m^2 s^{-1})	Tracer diffusivity (m^2 s^{-1})
NMTO	600 K	27.82	1.46×10^{-9}	2.13×10^{-10}
	700 K	49.42	2.61×10^{-9}	3.71×10^{-10}
	800 K	66.20	3.47×10^{-9}	7.98×10^{-10}
	900 K	124.68	6.56×10^{-9}	1.07×10^{-9}
NZTO	600 K	73.52	3.94×10^{-9}	5.67×10^{-10}
	700 K	85.70	4.59×10^{-9}	1.12×10^{-9}
	800 K	102.26	5.48×10^{-9}	1.40×10^{-9}
	900 K	133.59	7.15×10^{-9}	1.81×10^{-9}

Table S3. Optimized pristine interlayer spacing (d) of Mg-Mg, Mg-Te, Zn-Zn and Zn-Te, transitional interlayer spacing change (d'-d) in NEB calculations, and standard deviation of interlayer spacing in AIMD simulations at different temperatures of NMTO and NZTO, respectively.

		Pristine spacing (d, Å)	Interlayer spacing change in NEB (d'-d, Å)	Standard deviation of interlayer spacing in AIMD (Å)			
				600 K	700 K	800 K	900 K
NMTO	Mg-Mg	5.658	+0.086	0.090	0.103	0.114	0.122
	Mg-Te	5.658	+0.072	0.083	0.086	0.098	0.107
NZTO	Zn-Zn	5.672	+0.120	0.157	0.180	0.175	0.182
	Zn-Te	5.673	+0.096	0.129	0.139	0.141	0.148